Solid State Sciences 71 (2017) 3–7

Contents lists available at ScienceDirect

Solid State Sciences

journal homepage: www.elsevier.com/locate/ssscie

Crystallographic studies of $Ba_{12}Nb_{8-x}Ta_xCo_4O_{36}$ (x=1,3,4,5,7)

W. Wong-Ng [a], G. Liu [b, *], I. Levin [a], I. Williamson [c], A. Correa Hernandez [c], J.A. Kaduk [d], L. Li [c, e]

[a] Materials Measurement Science Division, National Institute of Standards and Technology, Gaithersburg, MD 20899, USA
[b] Science Research Institute, China University of Geosciences, Beijing 100083, China
[c] Micron School of Materials Science and Engineering, Boise State University, Boise, ID 83725-2090, USA
[d] Department of Chemical Sciences, Illinois Institute of Technology, Chicago, IL 60616, USA
[e] Center for Advanced Energy Studies, Idaho Falls, ID 83401, USA

ARTICLE INFO

Article history:
Received 7 April 2017
Received in revised form
17 June 2017
Accepted 21 June 2017
Available online 22 June 2017

Keywords:
X-ray diffraction patterns
Crystal structure
$Ba_{12}Nb_{8-x}Ta_xCo_4O_{36}$
Powder diffraction file (PDF)
TEM studies
Short-range 1:2 ordering

ABSTRACT

Crystal structures and X-ray reference powder diffraction patterns have been determined for the $Ba_{12}Nb_{8-x}Ta_xCo_4O_{36}$ (x = 1, 3, 4, 5, 7) series. $Ba_{12}Nb_{8-x}Ta_xCo_4O_{36}$ crystallize in the cubic perovskite structure with a space group $Pm\bar{3}\,m$ (No. 221) and the lattice parameter increasing from $a = 4.08732(3)$ Å to $a = 4.08894$ (2) Å as x varies from 1 to 7. The Goldschmidt distortion parameter for the entire series is about 1.05 (1.0488–1.0506), being similar to that of the cubic end member $Ba_3Nb_2CoO_9$. Transmission electron microscopy of the composition $Ba_{12}Nb_4Ta_4Co_4O_{36}$ (or $Ba_3(NbTaCo)O_9$) revealed nanoscale 1:2 ordering of Nb/Ta and Co, manifested in the presence of the diffuse superlattice reflections. As this ordering is limited to short range, the average structures were still refined assuming the ideal-perovskite cubic symmetry. X-ray powder diffraction patterns of the studied compounds have been submitted to the Powder Diffraction File (PDF).

1. Introduction

Continuing demand for environmentally friendly alternative energy technologies motivates intense research in energy conversion. The efficiency and performance of thermoelectric energy conversion or cooling is related to the dimensionless figure of merit (ZT) of the thermoelectric (TE) materials, given by $ZT = S^2\sigma T/\kappa$, where T is the absolute temperature, S is the Seebeck coefficient or thermoelectric power, σ is the electrical conductivity, and k is the thermal conductivity [1]. Low dimensional, layered oxides exhibit relatively high efficiencies for high-temperature waste-heat conversion applications. Examples of these oxides include cobaltates, such as $NaCoO_x$ [2], $Ca_2Co_3O_6$ [3,4], $Ca_3Co_4O_9$ [5–9], $Bi_2Sr_2Co_2O_x$ [10] and $Bi_{1-x}Pb_xOCuSe$ [11]. Thus, considerable research has been conducted to study various cobaltates for thermoelectric applications, including phase diagram studies of ternary oxide systems with CaO and Co_3O_4 as two of the end members [12–15].

Perovskite oxides, which a general formula ABO_3, have also attracted increasing attention in recent years as potential candidates for thermoelectric applications [16]. A number of these materials show reasonably high values of power factors. Perovskites are distinguished by their ability to simultaneously accommodate a wide range of species on both 12-fold coordinated A and 6-fold B cation sites. A mismatch between ionic sizes and radii for the cations sharing the same crystallographic sites provides a driving force for the ordering of these species. Common examples of ordered arrangements for the B cations correspond to the general stoichiometries $A_2BB'O_6$ and $A_3B_2B'O_9$ [17,18], which have been studied extensively. For example, Jacobson et al. [19] studied the series of $Ba_3B^{5+}{}_2B'^{2+}O_9$, where B=Ta and Nb, B' = Mg, Ni, Co, Zn, Mn, Ca, Sr, and Ba. However, they found that when B' = Ni, Co and Zn, the compounds remain disordered.

The present paper has two goals. First, the structures of $Ba_{12}Nb_{8-x}Ta_xCo_4O_{36}$ (x = 1, 2, 4, 5, 7) compounds are investigated for the effects of ionic size difference between Ta^{5+} and Nb^{5+}. Additionally, the X-ray diffraction patterns for $Ba_{12}Nb_{8-x}Ta_xCo_4O_{36}$ (x = 1, 2, 4, 5, 7) are measured to make them widely available as references through submission to the Powder Diffraction File (PDF [20,21]).

2. Experimental

2.1. Sample preparation

Both series of samples were prepared from stoichiometric amounts of $BaCO_3$, Nb_2O_5, Ta_2O_5, and Co_3O_4, using solid-state high-

* Corresponding author.
E-mail address: guangyaoliu@hotmail.com (G. Liu).

http://dx.doi.org/10.1016/j.solidstatesciences.2017.06.012
1293-2558/

temperature synthesis. The starting powders were mixed, pelletized, and calcined in air at 850 °C for 12 h, followed by subsequent annealing at 950 °C for 12 h, and at 1100 °C for a total of 44 h with intermediate grindings. During each heat treatment, the samples were furnace cooled. The heat treatment process was repeated until no further changes were detected in the powder X-ray diffraction patterns.

2.2. X-ray rietveld refinements and powder reference patterns[1]

The $Ba_{12}Nb_{8-x}Ta_xCo_4O_{36}$ (x = 1, 3, 4, 5, 7) compounds were mounted as ethanol slurries on a zero-background cell. The X-ray diffraction powder patterns were measured using a Bruker D2 Phaser diffractometer (30 kV, 10 mA, 5°–130° 2θ in 0.024° steps, 1 s/step) equipped with a LynxEye position-sensitive detector. For all samples, the lower window of the detector electronics was increased from its default value of 0.11 V–0.19 V to minimize the effects of fluorescence. All patterns (especially those from the sintered disks) show evidence of granularity.

The Rietveld refinement technique [22] with the software suite GSAS [23] was used to determine the structure of $Ba_{12}Nb_{8-x}Ta_xCo_4O_{36}$ (x = 1, 3, 4, 5, 7). Reference patterns were obtained using a Rietveld pattern decomposition technique. The reported peak positions were derived from the extracted integrated intensities, and positions calculated from the lattice parameters. For peaks that cannot be resolved, the intensities are summed, and an intensity-weighted d-spacing is reported.

2.3. Bond valence sum (BVS) calculations

The bond valence sum (*BVS*) values for the Ba, Nb, Ta, and Co sites were calculated using the Brown-Altermatt empirical expression [24,25]. The *BVS* of an atom *i* is defined as the sum of the bond valences v_{ij} of all the bonds from atoms *i* to atoms *j*. The most commonly adopted empirical expression for the bond valence v_{ij} as a function of the interatomic distance d_{ij} is $v_{ij} = \exp[(R_0 - d_{ij})/B]$. The parameter, *B*, is commonly assumed to be a "universal" constant equal to 0.37 Å. The values for the reference distances R_0 for Ba-O, Ta^{5+}-O, Nb^{5+}-O, Co^{2+}-O are (2.29, 1.920, 1.911, 1.692), respectively [24,25]. For crystallographic sites occupied by several types of atoms, the resulting BVS is calculated as the weighted sum according to site occupancies for the individual species.

2.4. Transmission electron microscopy (TEM)

TEM samples were prepared by crushing the powder in ethanol and dispersing the resulting suspensions on lacey-carbon-coated copper grids. The samples were examined in a Philips CM30 TEM operated at 200 kV.

3. Results and discussion

3.1. X-ray diffraction study

The results of Rietveld refinement for the $Ba_{12}Nb_{8-x}Ta_xCo_4O_{36}$ (x = 1, 2, 4, 5, 7) series are shown in Table 1 and Fig. 1. Table 1 gives various refinement statistical agreement factors whereas in Fig. 1, the observed (crosses), calculated (solid line), and difference XRD patterns (bottom) for $Ba_{12}Nb_4Ta_4Co_4O_{36}$ are illustrated; the difference pattern is plotted at the same scale. Above 60° 2θ, the vertical scale has been magnified by a factor of five. The row of tick marks indicates the calculated peak positions.

The structures of the $Ba_{12}Nb_{8-x}Ta_xCo_4O_{36}$ (x = 1, 3, 4, 5, 7) series are confirmed to be cubic (ideal ABO_3 perovskite), in agreement with previous reports by Jacobson et al. (1976). Table 2 lists the lattice parameters, which increase from a = 4.08732(3) Å to 4.08894 (2) Å with increasing x. The apparent disorder of Nb, Ta, and Co observed for $x \geq 1$ contrasts with the ordering of Nb and Co reported for the x = 0 member of these series, $Ba(Nb_{2/3}Co_{1/3})O_3$ [26]. Fig. 2 illustrates changes in the unit-cell volumes, *V*, in $Ba_{12}Nb_{8-x}Ta_xCo_4O_{36}$ (x = 1, 3, 4, 5, 7). *V* increases slightly (0.12%) across the entire solid solution series. Shannon [27] derived similar ionic radii of ≈0.64 Å for both Nb^{5+} and Ta^{5+}. Yet, recent evidence suggests that the effective radius of Ta is somewhat smaller than that of Nb. For example, measurements of extended X-ray absorption fine structure (EXAFS) in $Ag(Nb_{1/2}Ta_{1/2})O_3$ [28] revealed that the Nb-O distance is 1.99(1) Å compared to 1.96 Å for the Ta-O pair. Keller and Krämer [29] have also suggested that Ta^{5+} has a slightly smaller ionic radius (by −0.007 Å) than that of Nb^{5+}.

3.2. TEM results

Representative selected area electron diffraction in the ⟨110⟩ zone-axis orientation is shown in Fig. 3. The strong reflections are indexed according to the ideal cubic perovskite unit cell. The pattern reveals additional diffuse reflections at g = 1/3 $[111]^*$ (asterisk refers to a reciprocal space), which are indicative of short-range 1:2 ordering of Nb/Ta and Co on the octahedral sites, consistent with previous studies of $BaCo_{1/3}Nb_{2/3}O_3$. Two twin-variants having the ordering vectors aligned with the [111] and [11-1] directions contribute to the pattern. Dark-field imaging using these diffuse spots was challenging because of their weak intensity. However, considering the first-order nature of the disorder-1:2 order transition and judging from the diffuse streaking, the sample likely features nanoscale precipitates of the ordered phase having their habit planes perpendicular to the ordering vector, as has been observed previously in related systems. The pattern also seems to feature the diffuse blobs of intensity at ½$[111]^*$, which appear broader than might be expected from simple intersections of the diffuse streaks passing through 1/3$[111]^*$ reflections. These diffuse spots at ½$[111]^*$ could reflect the presence of 1:1 (rocksalt-type) ordered regions along with those exhibiting 1:2 order. Such coexistence of 1:1 and 1:2 ordered regions has been reported for the structurally-related $Ca_4Nb_2O_9$-$CaTiO_3$ system [30]. High-resolution TEM imaging is necessary to identity the exact nature of the ½$[111]^*$ diffuse maxima. As the cation order in these present samples is limited to short range, the ideal-perovskite cubic Pm3m symmetry is used to describe the average structure of the $Ba_{12}Nb_{8-x}Ta_xCo_4O_{36}$ series.

3.3. Structure of $Ba_{12}Nb_{8-x}Ta_xCo_4O_{36}$

The atomic coordinates, displacement parameters for the structures of $Ba_{12}Nb_{8-x}Ta_xCo_4O_{36}$ are given in Table 3. Figs. 4 and 5 illustrate the [110] projection and [001] projection of the crystal structure of $Ba_{12}Nb_{8-x}Ta_xCo_4O_{36}$, respectively, where the corner-sharing octahedra enclose the Ba-filled channels.

The stability of a perovskite compound with respect to distortions from the ideal cubic symmetry is commonly described using the Goldschmidt tolerance factor (t): $t = \langle r_A + r_O \rangle / \sqrt{2}\langle r_B + r_O \rangle$ [31], where $\langle r_A + r_O \rangle$ and $\langle r_B + r_O \rangle$ represent the average A-O and B-O distances, respectively, with $t = 1$ corresponding to the ideal cubic perovskite situation. As t approaches 1, the structure is expected to become less distorted; with $t < 1$ the distortion is accommodated by cooperative rotations of the $[BO_6]$ octahedra, reducing

[1] The purpose of identifying the equipment in this article is to specify the experimental procedure. Such identification does not imply recommendation or endorsement by the National Institute of Standards and Technology.

Table 1
Rietveld refinement residuals for $Ba_{12}Nb_{8-x}Ta_xCo_4O_{36}$, $Pm\bar{3}\ m$ (No. 221), $Z = 1$.

Composition		R_{wp}	R_p	χ^2
$Ba_{12}Nb_7TaCo_4O_{36}$	(x = 1)	0.0638	0.0485	1.19
$Ba_{12}Nb_5Ta_3Co_4O_{36}$	(x = 3)	0.0770	0.0574	1.20
$Ba_{12}Nb_4Ta_4Co_4O_{36}$	(x = 4)	0.0737	0.0548	1.25
$Ba_{12}Nb_3Ta_5Co_4O_{36}$	(x = 5)	0.0712	0.0536	1.22
$Ba_{12}NbTa_7Co_4O_{36}$	(x = 7)	0.0641	0.0488	1.20

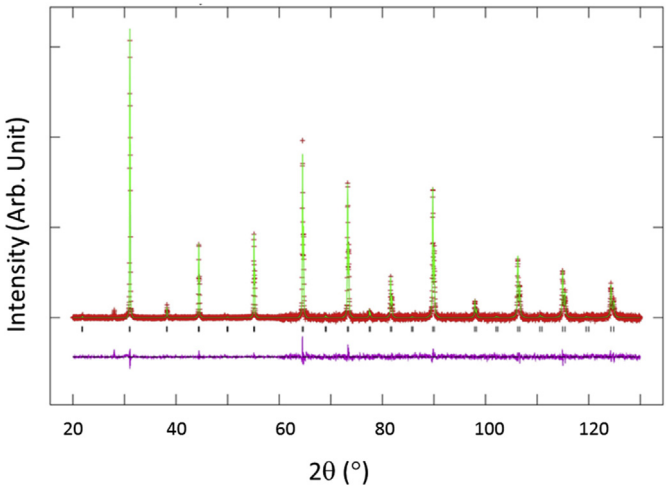

Fig. 1. Observed (crosses), calculated (solid line), and difference XRD patterns (bottom) for $Ba_{12}Nb_4Ta_4Co_4O_{36}$ by Rietveld analysis technique. The difference pattern is plotted at the same scale as the other calculated peak positions up to 60° 2θ. At higher angles, the scale has been magnified five times. The small peak in the 2θ° around 28° region is the K_β peak of the 110 reflection.

Table 2
Cell parameters and Goldschmidt tolerance factor '*t*' values [31] for $Ba_{12}Nb_{8-x}Ta_xCo_4O_{36}$, $Pm\bar{3}\ m$ (No. 221), $Z = 1$.

Chemical formula		*a*	*V*	d_{cal}	*t*
$Ba_{12}Nb_7TaCo_4O_{36}$	(x = 1)	4.08732(3)	68.283(1)	6.55	1.0488
$Ba_{12}Nb_5Ta_3Co_4O_{36}$	(x = 3)	4.08771 (3)	68.303(1)	7.27	1.0494
$Ba_{12}Nb_4Ta_4Co_4O_{36}$	(x = 4)	4.08787(3)	68.311(1)	7.20	1.0497
$Ba_{12}Nb_3Ta_5Co_4O_{36}$	(x = 5)	4.08810(2)	68.323(1)	7.38	1.0500
$Ba_{12}NbTa_7Co_4O_{36}$	(x = 7)	4.08894(2)	68.365(1)	7.73	1.0506

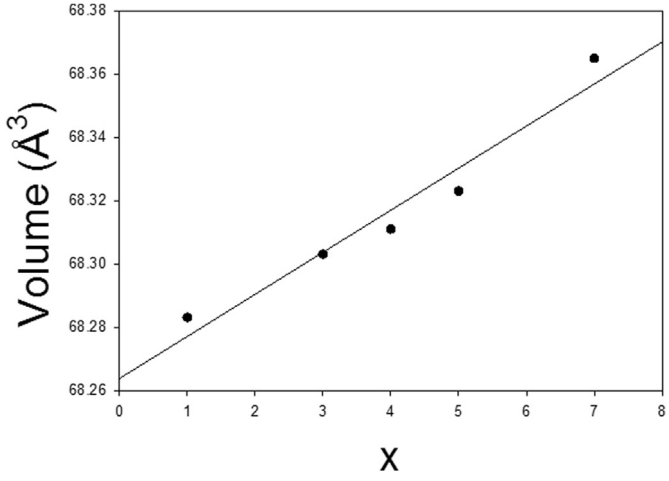

Fig. 2. Compositional dependence of the unit cell volume, *V*, for$Ba_{12}Nb_{8-x}Ta_xCo_4O_{36}$ A monotonic decrease of V is observed.

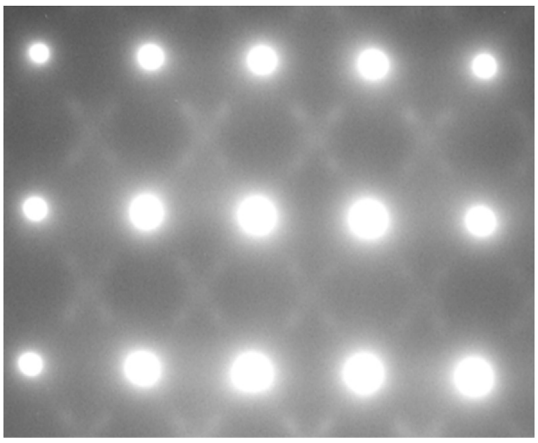

Fig. 3. A representative selected area electron diffraction pattern of a single grain in the $Ba_{12}Nb_4Ta_4Co_4O_{36}$ sample oriented with the ⟨110⟩ zone-axis parallel to the electron beam.

Table 3
Atomic coordinates and displacement factors for compounds for $Ba_{12}Nb_{8-x}Ta_xCo_4O_{36}$, $Pm\bar{3}\ m$ (No. 221), Z = 1.

Atom	*x*	*y*	*z*	Site Occ.	U_{iso}	Wyckoff symbol
$Ba_{12}Nb_7TaCo_4O_{36}$ (x = 1)						
Ba1	0	0	0	1.0	0.0054(4)	1a
Nb2	½	½	½	0.58333	0.0041(5)	1b
Ta3	½	½	½	0.08333	0.0041(5)	1b
Co4	½	½	½	0.33333	0.0041(5)	1b
O5	0	½	½	1.0	0.0069(15)	3c
$Ba_{12}Nb_5Ta_3Co_4O_{36}$ (x = 3)						
Ba1	0	0	0	1.0	0.0045(4)	1a
Nb2	½	½	½	0.41667	0.0058(5)	1b
Ta3	½	½	½	0.25	0.0058(5)	1b
Co4	½	½	½	0.3333	0.0058(5)	1b
O5	0	½	½	1.0	0.010(3)	3c
$Ba_{12}Nb_4Ta_4Co_4O_{36}$ (x = 4)						
Ba1	0	0	0	1.0	0.0049(5)	1a
Nb2	½	½	½	0.33333	0.0050(6)	1b
Ta3	½	½	½	0.33333	0.0050(6)	1b
Co4	½	½	½	0.33333	0.0050(6)	1b
O5	0	½	½	1.0	0.011(2)	3c
$Ba_{12}Nb_3Ta_5Co_4O_{36}$ (x = 5)						
Ba1	0	0	0	1.0	0.0044(5)	1a
Nb2	½	½	½	0.25	0.0058(6)	1b
Ta3	½	½	½	0.41667	0.0058(6)	1b
Co4	½	½	½	0.33333	0.0058(6)	1b
O5	0	½	½	1.0	0.009(2)	3c
$Ba_{12}NbTa_7Co_4O_{36}$ (x = 7)						
Ba1	0	0	0	1.0	0.0069(6)	1a
Nb2	½	½	½	0.08333	0.0035(6)	1b
Ta3	½	½	½	0.58333	0.0035(6)	1b
Co4	½	½	½	0.33333	0.0035(6)	1b
O5	0	½	½	1.0	0.0071(14)	3c

symmetry. The tolerance factor for all the presently studied compounds is around 1.05. Using the ionic radius of Ta computed by Keller and Kramer [29], the *t* values varies from 1.0488 to 1.0506 with x increasing from 1 to 7 (Table 2). These values are within the range typical for an undistorted cubic perovskite arrangement.

The bond distances and BVS values are summarized in Table 4. The Ba-O distances are chemically sound, ranging from 2.89017(2) Å for x = 1 to 2.89132(1) Å for x = 7, respectively, and the Nb/Ta/Co-O distance ranges from 2.04366(1) Å to 2.04447(1) Å for x = 1 to x = 7, respectively. From the BVS calculations, the coordination environment around the large A cation is somewhat compressed (cage too small) as the BVS values (from 2.172 to 2.166 with a small

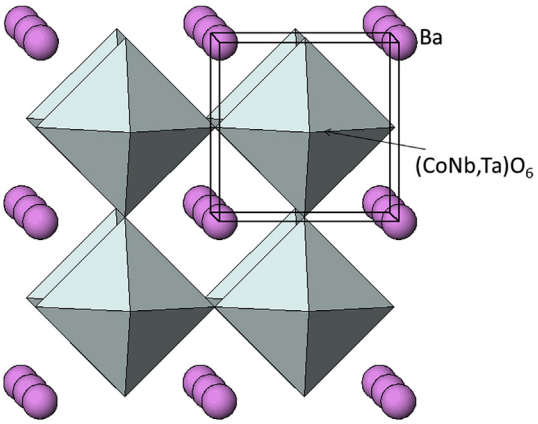

Fig. 4. A [110] projection of the crystal structure of $Ba_{12}Nb_{8-x}Ta_xCo_4O_{36}$ as derived from the X-ray powder data.

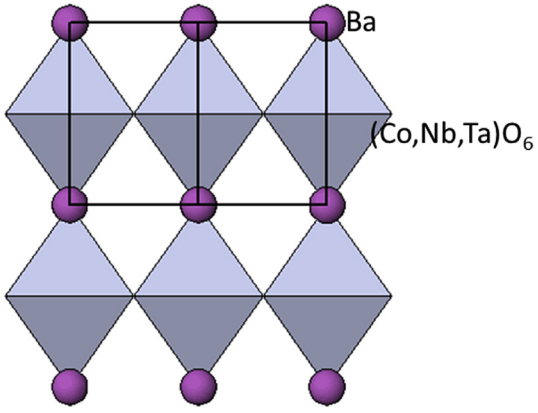

Fig. 5. A [001] projection of the crystal structure of $Ba_{12}Nb_{8-x}Ta_xCo_4O_{36}$ derived from the X-ray powder data.

amount of strain release as the amount of Ta^{5+} increases) are all greater than 2.0 (which is the ideal value for a strain-free Ba site). In contrast, the BVS values for the smaller (Nb/Ta/Co) sites indicate they are under tensile bond stress, as the BVS values (range from 3.576 to 3.620) are all smaller than the ideal average value of 4.0 for the B-site.

3.4. Reference x-ray diffraction pattern

An example of reference patterns for $Ba_{12}Nb_4Ta_4Co_4O_{36}$ (or $Ba_3(NbTaCo)O_9$) is given in Table 5. In these patterns, the symbols 'M′ and '+' refer to peaks containing contributions from two and more than two overlapping reflections, respectively. The peak that has the strongest intensity in the entire pattern is assigned an intensity of 999 and other lines are scaled relative to this value. In general, the d-spacing values are calculated from refined lattice parameters. The intensity values reported are integrated intensities

Table 5
X-ray powder pattern for $Ba_{12}Nb_4Ta_4Co_4O_{36}$, $Pm\bar{3}\,m$ (No. 221), $Z = 1$, $a = 4.08787(3)$ Å, $V = 68.311(1)$ Å^3, $D_x = 7.20$ g cm^{-3}. The symbols 'M′ refers to peaks containing contributions from two reflections, respectively. The particular peak that has the strongest intensity in the entire pattern is assigned an intensity of 999 and other lines are scaled relative to this value. The d-spacing values are calculated values from refined lattice parameters, and 'I' represents integrated intensity values.

d_{cal}	I_{obs}	h	k	l
4.0879	8	1	0	0
2.8906	999	1	1	0
2.3601	44	1	1	1
2.0439	299	2	0	0
1.8282	13	2	1	0
1.6689	384	2	1	1
1.4453	175	2	2	0
1.2927	155	3	1	0
1.2325	8	3	1	1
1.1801	51	2	2	2
1.0925	188	3	2	1
1.0220	29	4	0	0
0.9635	112	3	3	0 M
0.9635	112	4	1	1 M
0.9378	4	3	3	1
0.9141	97	4	2	0
0.8715	87	3	3	2

(rather than peak heights) based on the corresponding profile parameters as reported in Table 1. For resolved overlapped peaks, intensity-weighted calculated d-spacing, along with the observed integrated intensity and the *hkl* indices of both peaks (for 'M'), or the *hkl* indices of the strongest peak (for '+') are used. For peaks that are not resolved at the instrumental resolution, the intensity-weighted average d-spacing and the summed integrated intensity value are used. In the case of a cluster, unconstrained profile fits often reveal the presence of multiple peaks, even when they are closer than the instrumental resolution. In this situation, both d-spacing and intensity values are reported independently. All patterns have been submitted for inclusion in the Powder Diffraction File (PDF). The $Ba_{12}Nb_{8-x}Ta_xCo_4O_{36}$ (x = 1, 2, 4, 5, 7) patterns have been submitted for inclusion in the PDF.

4. Summary

Crystal structures and reference patterns of the $Ba_{12}Nb_{8-x}Ta_xCo_4O_{36}$ (x = 1, 2, 4, 5, 7) series of compounds have been determined and submitted to the Powder Diffraction File (PDF). According to X-ray powder diffraction, $Ba_{12}Nb_{8-x}Ta_xCo_4O_{36}$ adopts a simple perovskite structure. All the Ba sites have 12-fold coordination environment and all the mixed Co/Nb/Ta sites are 6-fold (octahedral) coordinated. TEM analysis of the $Ba_3(NbTaCo)O_9$ phase revealed short-range 1:2 ordering of Nb/Ta and Co on the octahedral sites. The slight changes in lattice parameters and the (Nb,Ta,Co)-O distances across the series might be related to the local cation ordering. The BVS values for the Ba sites (range from 2.172 to 2.166) indicate that the coordination environment around the large A site (in ABO_3 perovskite structure) is slightly compressive. On the other hand, the BVS values the smaller (Nb/Ta/Co) sites

Table 4
Bond distances and Bond Valence Sum (*BVS*) values for $Ba_{12}Nb_{8-x}Ta_xCo_4O_{36}$, $Pm\bar{3}\,m$ (No. 221), $Z = 1$. The ideal BVS values are 2.0 (Ba1 site), and 4.0 (mixed Nb2/Ta3/Co4 site), respectively. The values for the reference distance R_0 for Ba-O, Ta^{5+}-O, Nb^{5+}-O, Co^{2+}-O are 2.29, 1.920, 1.911, 1.692, respectively [24,25].

Atom	Atom	Bond Distances (Å) and BVS Values									
		(i)x = 1	*BVS*	(ii)x = 3	*BVS*	(iii)x = 4	*BVS*	(iv)x = 5	*BVS*	(v)x = 7	*BVS*
Ba1	O5x12	2.89017(2)	2.172	2.89044(1)	2.171	2.89056(1)	2.170	2.89072(1)	2.169	2.89132(1)	2.166
Nb2/Ta3/Co4	O5 x6	2.04366(1)	3.576	2.04385(1)	3.592	2.04393(1)	3.600	2.04405(1)	3.607	2.04447(1)	3.620

are under tensile bond stress.

Acknowledgement

ICDD is acknowledged for the grants-in-Aid assistance for the project. Also supported by “the Fundamental Research Funds for the Central Universities (Grant No. 2652015008)”, China.

References

[1] G.S. Nolas, J. Sharp, H.J. Goldsmid, Thermoelectric: Basic Principles and New Materials Developments, Springer, New York, 2001.
[2] I. Terasaki, Y. Sasago, K. Uchinokura, Large thermoelectric power in $NaCo_2O_4$ single crystals, Phys. Rev. B 56 (1997) 12685–12687.
[3] M. Mikami, R. Funahashi, M. Yoshimura, Y. Mori, T. Sasaki, High-temperature thermoelectric properties of single-crystal $Ca_3Co_2O_6$, J. Appl. Phys. 94 (10) (2003) 6579–6582.
[4] M. Mikami, R. Funahashi, The effect of element substitution on high-temperature thermoelectric properties of $Ca_3Co_2O_6$ compounds, J. Solid State Chem. 178 (2005) 1670–1674.
[5] D. Grebille, S. Lambert, F. Bourée, V. Petricek, Contribution of powder diffraction for structure refinements of aperiodic misfit cobalt oxides, J. Appl. Crystallogr. 37 (2004) 823–831.
[6] A.C. Masset, C. Michel, A. Maignan, M. Hervieu, O. Toulemonde, F. Studer, B. Raveau, Misfit-layered cobaltite with an anisotropic giant magnetoresistance: $Ca_3Co_4O_9$, Phys. Rev. B 62 (2000) 166–175.
[7] H. Mikami, K. Itaka, H. Kawaji, Q.J. Wang, H. Koinuma, M. Lippmaa, Rapid synthesis and characterization of $(Ca_{1-x}Ba_x)_3Co_4O_9$ thin films using combinatorial methods, Appl. Surf. Sci. 197 (2002) 442–447.
[8] Y.F. Hu, W.D. Si, E. Sutter, Q. Li, *In-situ* growth of c-axis- oriented Ca3Co4O9 thin films on Si(100), Appl. Phys. Lett. 86 (2005) 082103.
[9] W. Wong-Ng, Y.F. Hu, M.D. Vaudin, B. He, M. Otani, N.D. Lowhorn, Q. Li, Texture analysis of a $Ca_3Co_4O_9$ thermoelectric film on Si (100) substrate, J. Appl. Phys. 102 (3) (2007) 33520.
[10] S. Wang, A. Venimadhav, S. Guo, K. Chen, Q. Li, A. Soukiassian, D.G. Schlom, X.Q. Pan, W. Wong-Ng, M.D. Vaudin, D.G. Cahill, X.X. Xi, Structural and thermoelectric properties of $Bi_2Sr_2Co_2O_y$ thin films on $LaAlO_3$ (100) and fused silica substrates, Appl. Phys. Lett. 94 (2009) 022110.
[11] W. Wong-Ng, Y. Yan, J.A. Kaduk, X.F. Tang, X-ray powder diffraction reference patterns for $Bi_{1-x}Pb_xOCuSe$, Powder Diffr. 31 (3) (2016) 223–228.
[12] W. Wong-Ng, G. Liu, G.J. Martin, E.L. Thomas, N. Lowhorn, M. Otani, Phase compatibility of the thermoelectric compounds in the Sr-Ca-Co-O system, J. Appl. Phys. 107 (2010) 033508.
[13] W. Wong-Ng, T. Luo, M. Tang, M. Xie, J.A. Kaduk, Q. Huang, Y. Yang, M. Tang, T. Tritt, Crystal chemistry and thermoelectric properties of compounds in the Ca-Co-Zn-O system, J. Solid State Chem. 184 (8) (2011) 2159.
[14] W. Wong-Ng, W. Laws, Y.G. Yan, Phase diagram and crystal chemistry of the La-Ca-Co-O system, Solid State Sci. 17 (2013) 107–110.
[15] W. Wong-Ng, W. Laws, K.R. Talley, Q. Huang, J. Yan, J.A. Kaduk, Phase Equilibria and Crystal Chemistry of the CaO-$½Nd_2O_3$-CoO_z System at 885 °C in Air vol. 215, 2014, pp. 128–134.
[16] Y. Wang, Y. Sui, P. Ren, L. Wang, X. Wang, W. Su, H.J. Fan, Correlation between the structural distortion and thermoelectric characteristics in $La_{1-x}A_xCoO_3$ (A=Ca and Sr), Inorg. Chem. 49 (2010) 3216–3233.
[17] J.B. Goodenough, J.M. Longo, Landolt-bronstein, Crystallographic and Magnetic Properties of Perovskite and Perovskite Related Compounds, New Series, Group III vol. 4a, Springer-Verlag, New York, 1970.
[18] G. Blasse, New compounds with perovskite-like structures, J. Inorg. Nucl. Chem. 27 (1965) 993–1003.
[19] A.J. Jacobson, B.M. Collins, B.E.F. Fender, A powder neutron and x-ray diffraction determination of the structure of $Ba_3Ta_2ZnO_9$: an investigation of perovskite phases in the system Ba-Ta-Zn-O and the preparation of $Ba_2TaCdO_{5.5}$ and $Ba_2CeInO_{5.5}$, Acta Cryst. B32 (1976) 1083–1087.
[20] PDF, Powder Diffraction File, Produced by International Centre for Diffraction Data, 2015, 12 Campus Blvd., Newtown Squares, PA. 19073-3273, USA.
[21] W. Wong-Ng, H.F. McMurdie, C.R. Hubbard, A.D. Mighell, JCPDS-ICDD research associateship (cooperative program with NBS/NIST), J. Res. Natl. Inst. Stand Technol. 106 (6) (2001) 1013–1028.
[22] H.M. Rietveld, A profile refinement method for nuclear and magnetic structures, J. Appl. Cryst. 2 (1969) 65–71.
[23] A.C. Larson, R.B. von Dreele. General Structure Analysis System (GSAS), Los Alamos National Laboratory Report LAUR, Los Alamos, USA, 2004, pp. 86–748.
[24] I.D. Brown, D. Altermatt, Bond-valence parameters obtained from a systematic analysis of the Inorganic Crystal Structure Database, Acta Crystallogr. B 41 (1985) 244–247.
[25] N.E. Brese, and M. O'Keeffe, “Bond-valence parameters for solids,” Acta Crystallogr. B 47, 192–197.
[26] I. Molodetsky, P.K. Davies, Effect of $Ba(Y_{1/2}Nb_{1/2})O_3$ and $BaZrO_3$ on the cation order and properties of $Ba(Co_{1/3}Nb_{2/3})O_3$ microwave ceramics, J. Eur. Ceram. Soc. 21 (2001) 2587–2591.
[27] R.D. Shannon, Revised effective ionic radii and systematic studies of interatomie distances in halides and chalcogenides, Acta Crystallogr. A32 (1976) 751–767.
[28] I. Levin, J.C. Woicik, A. Llobet, M.G. Tucker, V. Krayzman, J. Pokorny, I.M. Reaney, Displacive Ordering Transitions in Perovskite-Like $AgNb_{1/2}Ta_{1/2}O_3$, Chem. Mater 22 (2010) 4987–4995.
[29] E. Keller, V. Krämer, Ionic' size differences from bond-valence parameters and from ionic radii, Acta Cryst. B62 (2006) 411–416.
[30] L.A. Bendersky, I. Levin, R.S. Roth, A.J. Shapiro, $Ca_4Nb_2O_9$-$CaTiO_3$: Phase equilibria and microstructures, J. Solid State Chem. 160 (2001) 257–271.
[31] V.M. Goldschmidt, Die Gesetze der Krystallochemie, Die Naturwiss. 14 (21) (1926) 477–485.